Journal of Cluster Science
https://doi.org/10.1007/s10876-018-1366-6

ORIGINAL PAPER

Encapsulation of Nickel Nanoparticles and Homopoly(Vinylsulfonic Acid) in Mesoporous Carbon CMK-3 as an Acid–Metal Bifunctional Catalyst for Tandem Reductive Amination

Roozbeh Javad Kalbasi[1] · Parisa Parishani[2] · Omid Mazaheri[2]

Received: 2 January 2018

Abstract
Facile and clean transformation for synthesizing secondary arylamines through one-pot reductive amination of aniline has been catalyzed by supported nickel nanocluster and poly(vinylsulfonic acid) into mesoporous carbon CMK-3 (Ni/PVSA/CMK-3) as a bi-functional metal/acid heterogeneous catalyst. Vinylsulfonic acid has been polymerized in CMK-3 pores by an in situ method. The process was run in the presence of $NaBH_4$ at room temperature, in a short reaction time, and without secondary product. Various characterization techniques, including FT-IR, XRD, TG, BET, SEM, TEM, DRS-UV, and AAS were employed to disclose the physical and chemical properties of the catalyst. Reaction results demonstrate that the optimized Ni/PVSA/CMK-3 catalyst shows comparable catalytic performance thanks to the nickel metals and the acidic nature of polymer incorporated in mesoporous channels of CMK-3. Besides being eco-friendly (using water as solvent), the method has several advantages such as simple work-up procedure and moderate to high-yield. This catalyst was easily filtered and reused without noticeable loss of activity after 10 runs.

Keywords One-pot reductive amination · Nickel nanoparticles · Poly(vinylsulfonic acid) · Acid–metal bifunctional catalyst

Introduction

Nowadays, amines are of great value with vast consumption in industries as intermediates for pharmaceuticals, biologically active compounds, rubbers, solvents, fine chemicals, dyes, herbicides, and in the manufacturing of detergents and plastics [1–3]. Reductive amination has been proved to be the versatile and appropriate procedure of amine synthesis [4, 5]. The reaction is comprised two steps including the formation of an imine during the reaction between primary amine and a carbonyl substrate, and the reduction of the imine with adequate hydride source [5]. There are two detached approaches for reductive amination: the direct approach, which uses the in situ-generated imine, and the indirect approach, which prior isolated imine is consumed [6]. The former method has several advantages such as one-pot procedure, high-yield simple setups, easy separation from the product, being stable and compatible reagents, and mild reaction conditions [7].

Many reports on reductive amination reaction with several different catalysts over the past decades have been presented. Among them, heterogeneous catalysis is more convenient than homogenous catalysis because of separation and recovery capabilities [8]. Moreover, it has been proven that two characters of metallic and acidic are necessary to perform this reaction; consequently, acid–metal bi-functional heterogeneous catalysts are frequently used in this reaction [9].

Recently, several metal nanoparticles such as Ag, Ni, Cu, and Pd acted as a hydride transfer [10, 11]. Consuming Ni and Cu in catalytic purpose are economically more feasible since nickel and copper are cheaper than precious metals like Ag, Au, Pd, and Pt. Ni^0 activity is much weaker than other metals like Pd^0 and Au^0. Thus, finding a procedure to intense metal activity is essential. Nickel nanoparticles or cationic nickel complexes have been used

✉ Roozbeh Javad Kalbasi
rkalbasi@gmail.com; rkalbasi@khu.ac.ir

[1] Faculty of Chemistry, Kharazmi University, Tehran, Iran

[2] Department of Chemistry, Shahreza Branch, Islamic Azad University, 311-86145, Isfahan, Iran

Published online: 26 March 2018

as hydrogen-transfer agent in reductive amination reactions [12, 13]. However, using lithium and base in harsh conditions such as high temperature, toxic solvents and long reaction time in these reactions were the most drawbacks.

Furthermore, despite a fruitful particle size monitoring and a uniform distribution of nanoparticles are generally predicted in catalytic applications, nanoparticles distinctively accumulate together in bulk materials, which decline the activity and the selectivity of catalysts. To overcome this problem, mesoporous silica, zeolites, polymers or macromolecular organic ligands have been used in order to immobilize metal nanoparticles in their pores [14, 15]. Mesoporous silica materials and zeolites have great order and surface area than other materials like polymer, etc.; subsequently, they are appropriate for catalysis approaches [16, 17].

Lately, mesoporous silica was used to produce mesoporous carbon (CMK-n) as a hard template [18]. These materials have several advantages compared to mesoporous silica and zeolites like superb stability in strong acids and bases conditions, high mechanical and thermal stability in the nitrogen atmosphere and other engrossing properties such as narrow pore size distributions, high surface areas, and ordered structures [19]. In addition, mesoporous carbon materials have hydrophobic nature on their surfaces where nanopolymers can be entirely embedded in their pores [20]. Consequently, mesoporous carbon can be greatly effective to maximize the nickel activity due to the distribution of the nickel nanoparticles into the mesostructures.

In our previous studies, it asserts that by modification of mesoporous materials surfaces using functional polymers, their functionalities become perfect. In brief, by this way, the polymers have a smaller particle size and subsequently higher surface areas. Thus, polymer chains fit in the pores, and could not leach from the pores of mesoporous structure. Here, CMK-3 replicating from mesoporous silica (SBA-15) was prepared and applied as a support for nickel nanoparticles and poly(vinylsulfonic acid) (Ni/PVSA/CMK-3). The one-pot reductive amination reaction has been accomplished using aldehyde with 6 mmol $NaBH_4$ in two different kinds of solvent including water and acetonitrile at 25 °C without any by-products. The homopolymer acts as an acid site in order to carbonyl activation and Ni nanoparticle acts as a hydride transfer. Besides, TOF and TON were calculated to demonstrate the nickel activity in reductive amination reaction.

Experimental Method

Materials and Catalyst Characterization

All chemicals were purchased from Merck and Sigma-Aldrich and used as received. Samples including pre-catalysts, catalyst, and synthesized products were analyzed by Fourier Transform Infrared Spectroscopy (using a PerkinElmer 65 in KBr matrix in the range of 4000–400 cm^{-1}). The thermal gravimetric analysis (TGA) data were acquired by the STA with 10 °C min^{-1} heating rate in 30–650 °C and in ambient nitrogen. The X-ray powder diffraction of the samples was fulfilled by the Bruker D8Advance X-ray having Ni-filtered and Cu Kα radiation at 40 kV. Adsorption–desorption of nitrogen at liquid nitrogen temperature was used by BEL SORP 18 to establish the BET specific surface areas and BJH pore size distribution. The amount of nickel was determined by atomic absorption spectrophotometer, Perkin Elmer AAnalyst 300 model. SEM and TEM studies were conducted by Philips, XL30 model and JEOL JEM.2011, 200.00 kV, respectively. The DRS UV–vis spectra were indicated with JASCO spectrometer, the V-670 model. Moreover, the final products were identified by ^{1}H NMR and ^{13}C NMR spectra (Bruker DRX-500 Avance spectrometer at 500 and 125 MHz, respectively). An Electrothermal 9100 apparatus are measured secondary amines melting points and it aligned and compared with previous reports.

Catalyst Preparation

Preparation of Mesoporous Carbon (CMK-3)

Employed mesoporous carbon (CMK-3) was synthesized following the method reported by Ryoo applying SBA-15 as a high order silica template [21].

Mesoporous silica SBA-15 was prepared by using Pluronic P123 ($EO_{20}PO_{70}EO_{20}$) block copolymer as the template and tetraethylorthosilicate (TEOS) as the silica source by way of adding H_3PO_4 [22]. In a general procedure, P123 (2 g) was dissolved in deionized water (75.4 mL) at 25 °C and H_3PO_4 (4.2 mL, 85%). After that, TEOS (4.6 mL) was added to the solution and the polymerization was fulfilled by mixing at 35 °C for 24 h in the sealed Teflon breakers. Consequently, the mixed solution placed at boiling point for 1 day. Afterward, in order to separate P123/SBA-15, the solution was filtered and washed several times with water. In the end, the P123/SBA-15 was dried at 100 °C overnight. Owing to remove the P123, the P123-SBA-15 was calcined at 250 °C and 550 °C for 3 and 4 h, respectively, in an air atmosphere.

Then, mesoporous carbon CMK-3 was produced using SBA-15 and sucrose as template and carbon source, respectively. At first, 1.25 g (3.65 mmol) sucrose and 0.14 g (1.42 mmol) of H_2SO_4 (98%) and 1.0 g SBA-15 alternatively were added to 5 ml deionized water. The mixture was heated at 100 °C and 160 °C for 6 h and another 6 h, respectively. In the second stage, in order to adequate polymerization inside the SBA-15 pores, 5 ml

aqueous solution containing 0.8 g (2.33 mmol) sucrose and 0.09 g (0.917 mmol) of H_2SO_4 was added again. Then, the black material was exposed to the thermal schedule explaining above, one more time. Afterward, the solid black material was carbonized under nitrogen gas flow at 900 °C for 6 h with a heating rate of 5 °C min^{-1}. In order to remove silica, the material was washed with 1 M sodium hydroxide solution in 50 vol% ethanol-50 vol% H_2O. Eventually, the solid was filtered and washed with ethanol and dried at 100 °C for 4 h.

Preparation of Poly(Vinylsulfonic Acid)/CMK-3

To start polymerization, 1.2 g vinylsulfonic acid sodium salt solution (25 wt% in H_2O) was converted into its acidic form using the ion exchange resin (Amberjet 1200 H, 2 equiv. L^{-1}, Aldrich). After that, the monomer and 0.2 g of CMK-3 were mixed in 5 mL water in a round bottom flask. 0.0024 g potassium persulfate (KPS) and 0.001 g sodium bisulfite (SBS) were added and the mixture was stirred for 1 day at 25 °C in the nitrogen atmosphere. The black solid (PVSA/CMK-3) was filtered and dried at 60 °C. According to the TGA results, the yield of polymerization was 90%. Moreover, the number of acidic sites, which relates to poly(vinylsulfonic acid) was evaluated by potentiometric titration. The acidic site content was 4 mmol g^{-1}.

Preparation of Ni Nanoparticle on Poly(Vinylsulfonic Acid)/CMK-3

Ni/PVSA/CMK-3 was synthesized as follows: 0.1 g of PVSA/CMK-3 was added to 3 mL water and 1 mL of nickel chloride hexahydrate (0.5 M). The mixture was heated for 4 h at 80 °C. Next, the $NaBH_4$ solution [0.057 g (1.5 mmol)] in 5 mL methanol was added to the mixture drop by drop in 10 min. Then, the solution was stirred for 3 h. After that, the same amount of $NaBH_4$ was added and the mixture was stirred up for another 3 h. Consequently, after filtering and washing the solution with methanol/water (50–50%), the mixture was dried at 25 °C to yield Ni/PVSA/CMK-3 (Scheme 1). To estimate the amount of Ni, the catalyst (Ni/PVSA/CMK-3) was decomposed by perchloric acid, nitric acid, fluoric acid and hydrochloric acid. The Ni content was 1.9 mmol g^{-1} (AAS estimating).

One-Pot Reductive Amination Procedure

In a round bottom flask, 2 mmol Aniline and 2 mmol Benzaldehyde were mixed for one min at 25 °C into 3 mL water or Acetonitrile as a solvent. Afterward, to accomplish the reaction, 0.04 g (3.8 mol% Ni and 8 mol% acid sites) catalyst (Ni/PVSA/CMK-3) and 6 mmol $NaBH_4$ were added to the reactants. During the reaction, the benzaldehyde was monitored by TLC at 25 °C until the benzaldehyde completely disappeared. Next, the product was

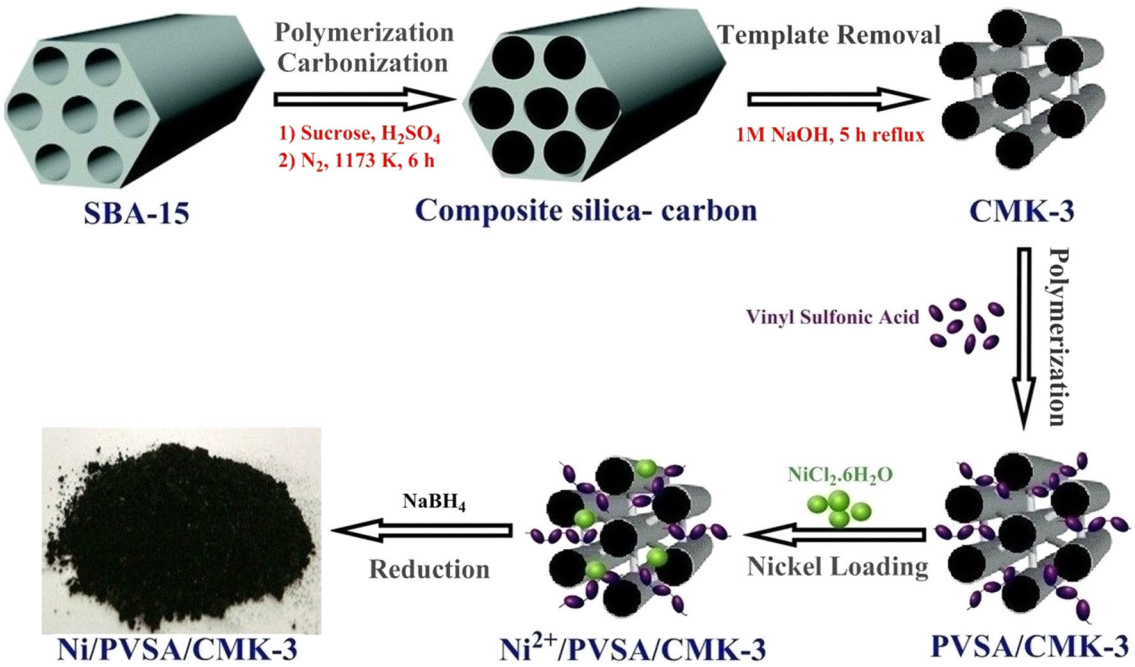

Scheme 1 Preparation of Ni/PVSA/CMK-3

washed with 10 mL water and subsequently, it was extracted by diethylether. After that, the anhydrous Na_2SO_4 was used as a drying agent. Finally, the products were purified just by diethylether extraction in the majority of the reactions and the isolated yields were determined.

Results and Discussion

Catalyst Characterization

The images of the FT-IR spectra of CMK-3 (a), PVSA/CMK-3 (b) and Ni/PVSA/CMK-3 (c) are presented in Fig. 1. All samples show a broad band at around 3380–3470 cm^{-1} due to the O–H stretching vibration of adsorbed water molecules [23]. In the CMK-3 spectrum, no signals of organic bonds are observed, indicating complete carbonization of sucrose (Fig. 1a) [24]. The presence of new peaks at 1041 and 1186 cm^{-1} are attributed to the S=O group of PVS, confirming the existence of the grafted PVSA chains into the CMk-3 [25]. The peak around 960 cm^{-1} is absent in PVSA/CMK-3, which confirms the elimination of C=C bond. Moreover, the existence of absorption bond at around 2940 and 1450 cm^{-1} correspond to the aliphatic C–H stretching and bending of PVSA, respectively, (Fig. 1b) [26]. The appearance of the above bands reveals that PVSA has been incorporated into the carbon mesoporous and the synthesis of PVSA/CMK-3 has been succeed. The characteristic bands in Ni-PVSA/CMK-3 spectrum are broadened after adding Ni nanoparticles. This is due to the interaction between Ni particles and sulfonic acid groups.

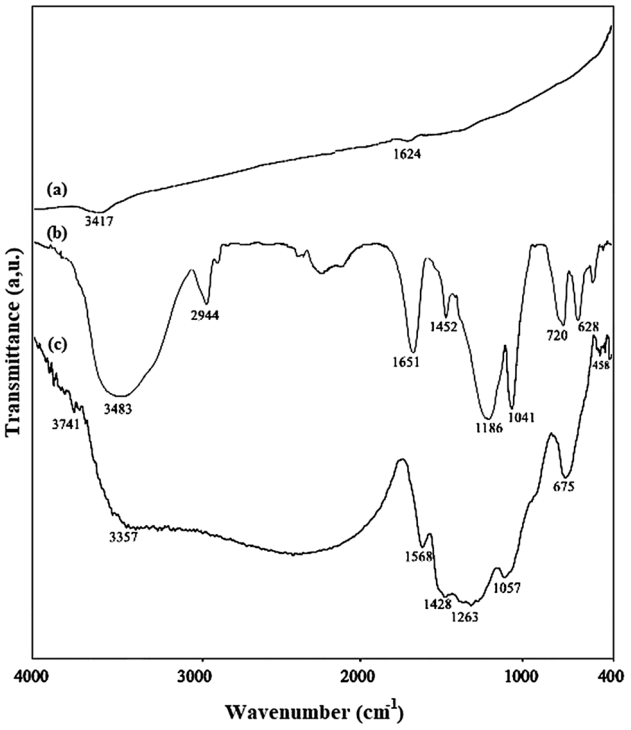

Fig. 1 FT-IR spectra of CMK-3 (*a*), PVSA/CMK-3 (*b*) and Ni/PVSA/CMK-3 (*c*)

The profiles of thermo gravimetric analysis of PVSA, PVSA/CMK-3 and Ni/PVSA/CMK-3 subject the nitrogen atmosphere are shown. As observed in Fig. 2, decomposition process of PVSA begins at around 150 °C and continues up to 300 °C; from 300 to 500 °C, a slight decomposition take place. This observation indicates that Poly(vinylsulfonic acid) cannot tolerate high temperatures since the polymers are not protected by support materials [27]. The TGA curve of PVSA/CMK-3 in 150–330 °C range shows a slight mass loss (5%, w/w approximation), which is associated with the degradation of SO_2 and ethylene from PVSA (Fig. 2) [28]. One great's stage of PVSA degradation occurs at temperatures above 330 °C. PVSA mass lose in the same stage is 49% (w/w), attributed to methane deterioration [28]. By comparing PVSA and PVSA/CMK-3 curves, it is clear that PVSA/CMK-3 has slower degradation rate and higher thermal stability in comparison to PVSA. Hence, after hybridization, the thermal stability is significantly elevated to a point that where it can be beneficial for catalysis applications. In addition, the TGA of Ni/PVSA/CMK-3 shows two mass loss detachments steps that it is almost similar to that of the PVSA/CMK-3. At this stage, the temperature between 330 °C and 445 °C is the only difference at which Ni/PVSA/CMK-3 shows slower degradation rate than PVSA/CMK-3. The Ni/PVSA/CMK-3 has shown slightly higher thermal stability than PVSA/CMK-3. This phenomenon might be related to the nickel nanoparticles, available in the meso-structure [29, 30].

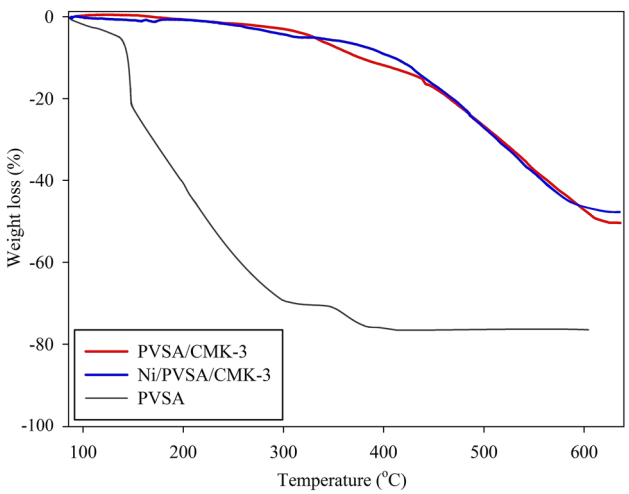

Fig. 2 TGA curves of PVSA, PVSA/CMK-3, and Ni/PVSA/CMK-3

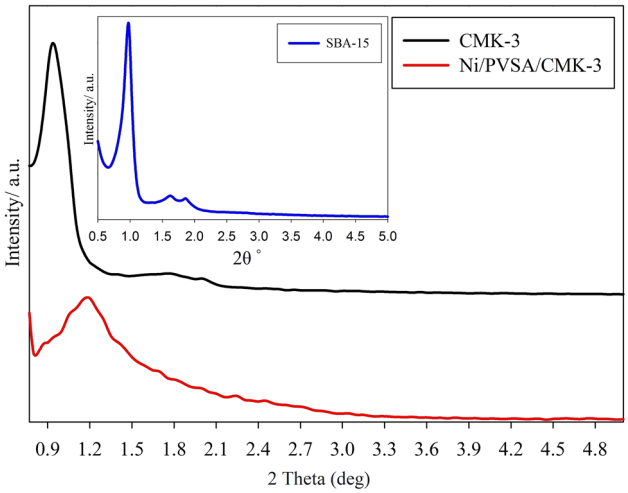

Fig. 3 XRD patterns of CMK-3, and Ni/PVSA/CMK-3 (2θ = 0.5–5). Inside: SBA-15 (2θ = 0.5-5)

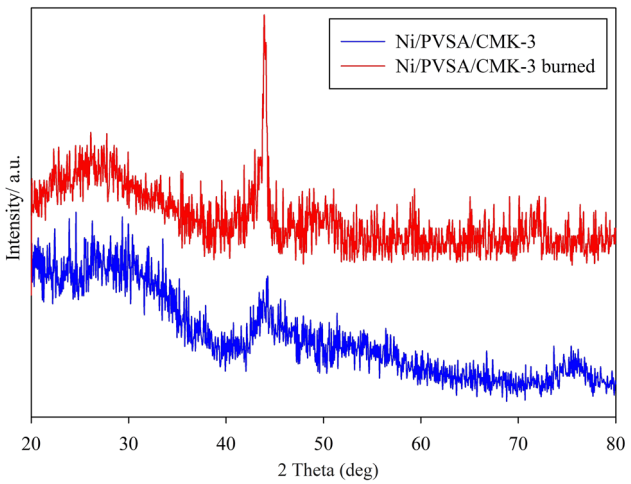

Fig. 4 XRD patterns of amorphous Ni/PVSA/CMK-3 and Ni/PVSA/CMK-3 burned in 400 °C for 4 h (2θ = 20–80)

The XRD patterns of SBA-15, CMK-3, and Ni/PVSA/CMK-3. SBA-15 have one strong peak at 2θ = 0.5° and two weak peaks within 2θ values from 0.5° and 2° assigning to (100), (110), and (200) diffraction, respectively; which corresponds to the well-known-ordered arrangement of SBA-15 in the space group *p6mm* of 2-D hexagonal symmetry (Fig. 3, inside) [21]. The silica SBA-15 was applied as a template to produce CMK-3. As can be seen, the XRD pattern of CMK-3 shows three diffraction peaks at 2θ = 1.04°, 1.79°, and 2.05°, (Fig. 3), which could be assigned to (100), (110) and (200) diffraction of the 2D hexagonal space group *p6mm* [21].

After polymerization of vinylsulfonic acid and immobilizing nickel, the XRD of Ni/PVSA/CMK-3 reveals the identical pattern of CMK-3. This phenomenon indicates that the structure of the CMK-3 is preserved even after polymerization (Fig. 3). However, the intensity of the characteristic reflection peaks of the Ni/PVSA/CMK-3 is diminished (Fig. 3). The composite contains less CMK-3 due to the dilution of the CMK-3 with PVSAs and Ni nanoparticles; subsequently, this dilution could be responsible for a decrease the peak intensity [30]. In addition, in Ni/PVSA/CMK-3, the chief peak shifts to greater 2θ (in comparison with CMK-3). According to the Bragg's law, an increase in 2θ makes the d spacing smaller, which might be related to the entrance of poly(vinylsulfonic acid)s and nickel nanoparticles into the layers of mesoporous carbon CMK-3. This finding is precisely compatible with the BET results. In general, the XRD patterns of CMK-3 and Ni/PVSA/CMK-3 are almost similar to the SBA-15, showing that the CMK-3 is an accurate replica of the mesoporous silica SBA-15. Here, the polymerization and embedding nickel nanoparticle process do not drastically destruct the CMK-3 structure.

After immobilizing nickel in the PVSA/CMK-3, only one amorphous pattern at around 2θ = 44° (Fig. 4) is observed and the Ni peak cannot be discerned because of the homogeneity of nickel nanoparticles. To demonstrate

Table 1 Physicochemical properties of CMK-3, PVSA/CMK-3 and Ni/PVSA/CMK-3 samples obtained from N_2 adsorption–desorption

Sample	$S_{mesopore}$ ($m^2\ g^{-1}$)[a]	$V_{mesopore}$ ($cm^3\ g^{-1}$)[a]	$D_{mesopore}$ (nm)[a]	$D_{mesopore}$ (nm)[b]	$S_{micropore}$ ($m^2\ g^{-1}$)[c]	$S_{mesopore}$ ($m^2\ g^{-1}$)[c]	$V_{micropore}$ ($cm^3\ g^{-1}$)[c]	$D_{micropore}$ (nm)[c]	$S_{micropore}$ ($m^2\ g^{-1}$)[d]	$S_{mesopore}$ ($m^2\ g^{-1}$)[d]
CMK-3	1486	1.1	4.1	3.19	–	–	–	–	–	–
PVSA/CMK-3	521	0.64	4.95	3.28	67	408	0.3	1.2	90	515
Ni/PVSA/CMK-3	420	0.52	4.92	3.28	56	344	0.3	1.2	65	421

[a]Calculated by BET method

[b]Mean pore diameter determined by using BJH method from the adsorption branch of the isotherm curves

[c]Calculated by MP-Plot method

[d]The micropore surface area was estimated by the t-plot analysis using the adsorption branch of the isotherm curves

the Ni nanoparticles presence in the Ni/PVSA/CMK-3, the catalyst was exposed to 400 °C. Meanwhile, a higher intensity peak at $2\theta = 44°$ appears due to converting the amorphous Ni phase into the crystalline phase, which relates to the small size of the nickel nanoparticles and the plane (111) of *fcc* nickel [17].

The specific surface area, pore volume and the pore size of the CMK-3, PVSA/CMK-3, and Ni/PVSA/CMK-3 samples were asserted by BET, BJH, MP-Plot, and t-Plot methods, Table 1. Nitrogen sorption isotherms of PVSA/CMK-3 and Ni/PVSA/CMK-3 specimens are illustrated in Fig. 5. Both samples demonstrate type IV adsorption isotherm with a H1 hysteresis loop at a pressure around 0.3–0.7 (Fig. 5). The appropriate incorporation of the poly(vinylsulfonic acid) and nickel nanoparticles into the CMK-3 pores makes the PVSA/CMK-3 and Ni/PVSA/CMK-3 to exhibit smaller pore volume and the specific surface area in those of CMK-3 juxtaposition (Table 1). As can be seen, pore diameter increases in the PVSA/CMK-3 and Ni/PVSA/CMK-3 in comparison with that of the CMK-3. This phenomenon reveals that the incorporation of polymer chains, at their growth, producing a pressure (the physical pressure on the channels' wall) inside the CMK-3 mesopores [31, 32]. By adding Ni nanoparticles into PVSA/CMK-3, the specific surface area and pore volume are diminished (calculated by BET, MP-plot, and t-plot) indicating that nickel nanoparticles are located inside the CMK-3 pores. Despite the significant decrease in pore volume and surface area, the Ni/PVSA/CMK-3 pores are not obstructed by nickel nanoparticles and homopolymer precipitation.

The BJH pore size distribution curves of the PVSA/CMK-3 and Ni/PVSA/CMK-3 reveal a thin pore size distribution (Fig. 6), indicating that homopolymer and nickel nanoparticles are distributed into the CMK-3 pores in an appropriate manner. This result is in agreement with TEM

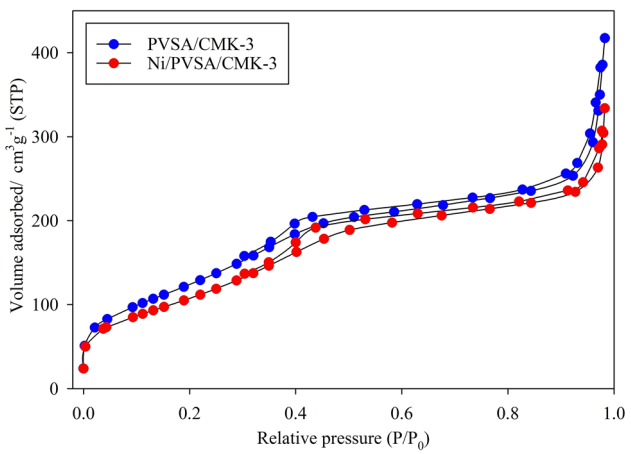

Fig. 5 N_2 adsorption/desorption isotherms of PVSA/CMK-3 and Ni/PVSA/CMK-3

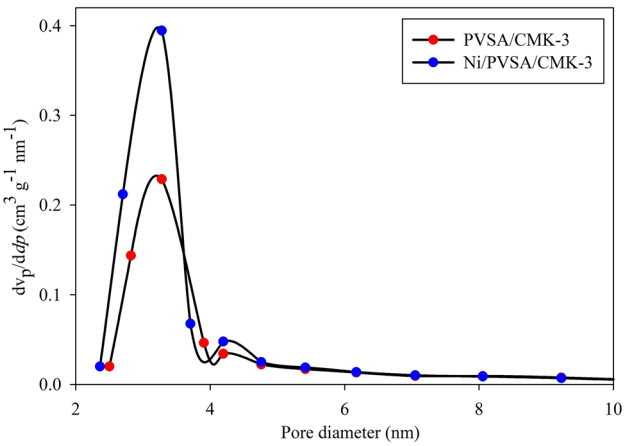

Fig. 6 Pore size distributions of PVSA/CMK-3 and Ni/PVSA/CMK-3 obtained by BJH method

survey, revealing that the polymer chains have a functional role in nickel nanoparticles entrapment and dispersion.

The SEM images of CMK-3, PVSA/CMK-3, and Ni/PVSA/CMK-3 are presented in Fig. 7, where all have rod-like morphology, which is attributed to carbon mesoporous [33]. Although no notable difference is observed in surface morphology between CMK-3 and PVSA/CMK-3, it is evident that after hybridization, the CMK-3 surface becomes coarser. It indicates that the most polymerization of PVSA takes place in the CMK-3 pores. In addition, this phenomenon is justified through a reduction in surface area and pore volume, Table 1. Due to immobilizing the Ni nanoparticles, several spherical beads on the surface of mesoporous carbon are observed in Fig. 7. On the contrary, most of them are incorporated into the carbon mesoporous CMK-3 structure, non-visible in the SEM images. It is notable that after loading nickel nanoparticles into the CMK-3, the structure of the mesoporous carbon remains intact; this claim is confirmed by both XRD analysis and TEM images.

The PVSA/CMK-3 and Ni/PVSA/CMK-3 were inspected by the means of TEM micrographs technique, (Fig. 8). The ordered mesostructure of PVSA/CMK-3 and Ni/PVSA/CMK- 3 which specifies the ordered-structure of mesoporous carbon is retained with ~ 5–6 nm even after polymerization and incorporation of PVSA and Ni nanoparticles, respectively. These findings confirm what the BET results show. The larger darker spots indicate the existence of Ni nanoparticles with different distributions (Fig. 8c). Moreover, the larger dark spots are shown in Fig. 8d, which are corresponded to Ni nanoparticles agglomerated on the exterior surface with ~ 6–9 nm average diameter. As observed, the small dark spots could be attributed to nickel nanoparticles with ~ 4–6 nm average diameter, presumably located in the mesoporous channels.

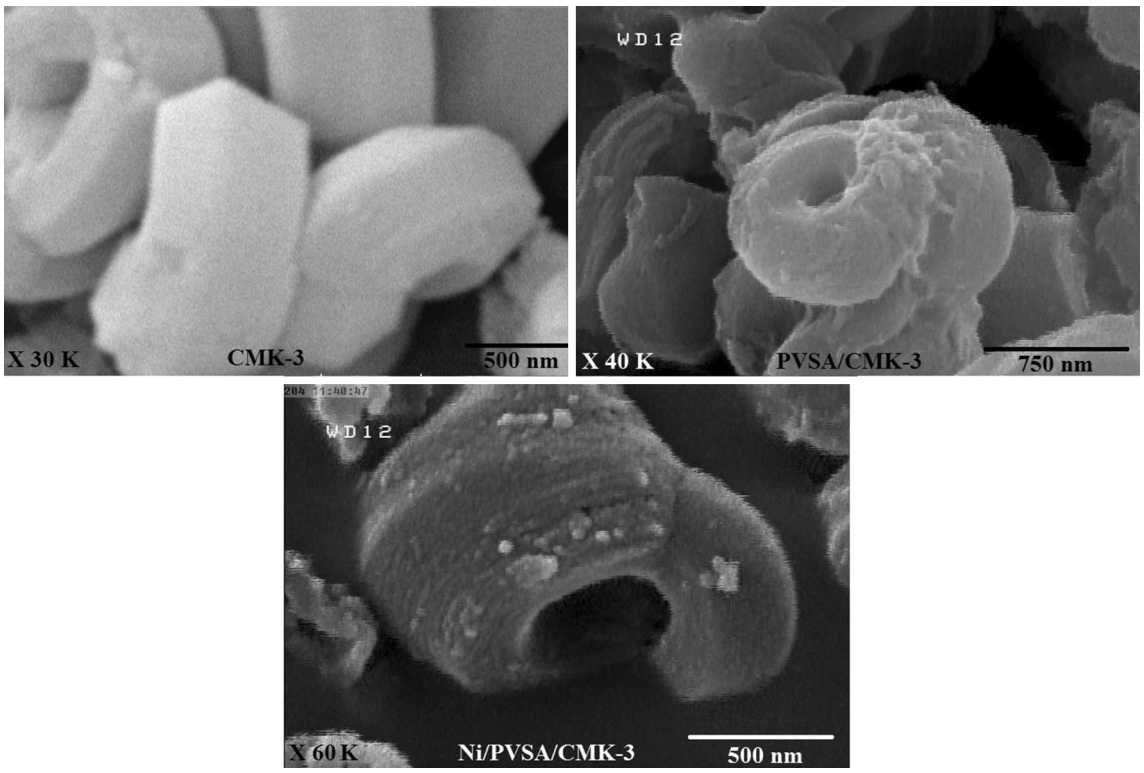

Fig. 7 Scanning electron microscopy (SEM) photographs of CMK-3, PVSA/CMK-3, and Ni/PVSA/CMK-3

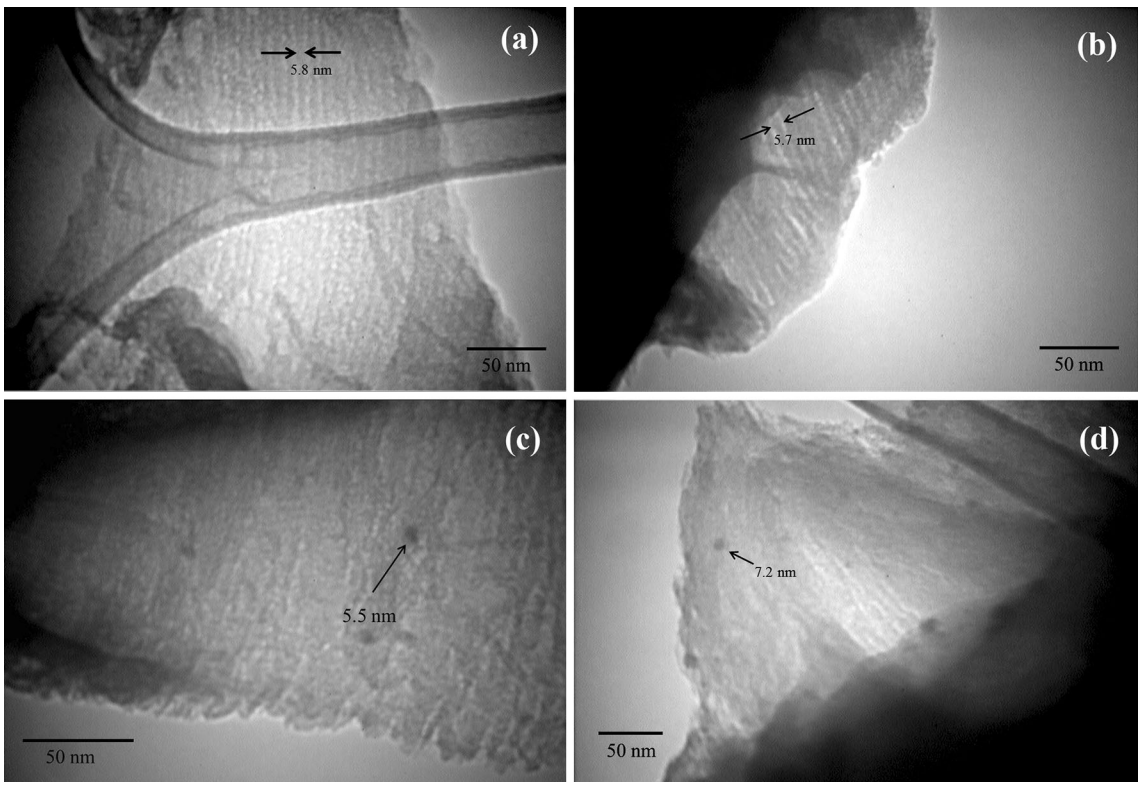

Fig. 8 Transmission electron microscopy (TEM) of **a**, **b** PVSA/CMK-3 and **c**, **d** Ni/PVSA/CMK-3

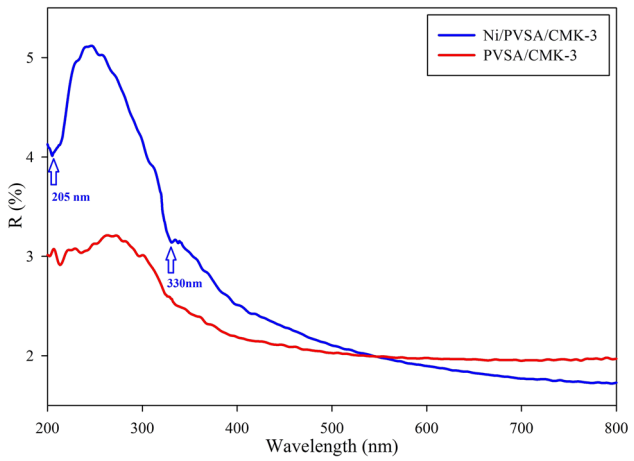

Fig. 9 DRS-UV spectra of PVSA/CMK-3 and Ni/PVSA/CMK-3

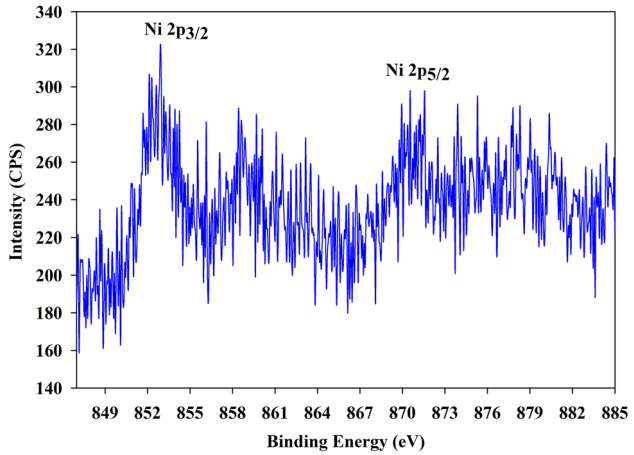

Fig. 10 XPS spectrum of Ni2p of Ni/PVSA/CMK-3

The DRS-UV of PVSA/CMK-3 and Ni/PVSA/CMK-3 are exhibited in Fig. 9. The previous study is proven that DRS-UV of the cationic nickel has two d–d transitions peaks of $^3T_{1g}(P) \leftarrow {}^3A_{2g}$ (F) (368 nm) and $^3T_{1g}$ (F) $\leftarrow {}^3A_{2g}$ (F) (576 nm) [34], which is not observed in Ni/PVSA/CMK-3. Moreover, the DRS-UV of Ni/PVSA/CMK-3 shows features bands of around 205 and 330 nm, which are assigned to the Ni nanoparticles in this sample [35]. By comparing these data, it can be found that cationic nickels are successfully converted into nickel nanoparticles by $NaBH_4$.

Figure 10 shows the XPS spectrum of Ni/PVSA/CMK-3 obtained from the reduction of Ni^{2+} by sodium borohydride. The Ni2p spectrum with the binding energies of $Ni2p_{3/2}$ and $Ni2p_{1/2}$ lying at about 852.9 and 870.4 eV, respectively is related to Ni nanoparticles with metallic state [36–38]. However, standard binding energy of Ni^0 in $Ni2p_{3/2}$ shows 852.3 and 870.5 eV for $Ni2p_{1/2}$ [36, 37]). It can be concluded that the Ni peaks in Ni/PVSA/CMK-3 slightly shifted to higher binding energy than Ni^0 standard binding energy. As we know, the position of Ni2p peak is usually influenced by the local chemical/physical environment around Ni species besides the formal oxidation state, and shifts to higher binding energy when the charge density around it decreases [38]. Consequently, the existence of the acidic sites of $–SO_3H$ (with the electron withdrawing nature) around the Ni^0 species leads to a decrease in the charge density around Ni^0 and the slight increase in binding energy [39].

Catalytic Activity

Over two decades, many assessments have been devoted to develop environment-friendly synthesis. What is really noticeable in sustainable chemistry is consuming water as a reaction medium in transition metal-catalyzed processes [40]. Water has the environmental and economic sense owing to a non-toxic solvent, plenty easily accessed, inexpensive, and non-inflammable [41]. Accordingly, the effect of several factors in the one-pot tandem reductive amination of aldehydes with aniline by consuming Ni/

Table 2 Effect of $NiCl_2{\cdot}6H_2O$ molar ratio on the catalytic activity

Entry	$NiCl_2{\cdot}6H_2O$ (mmol g^{-1})	Ni content of catalyst (mmol g^{-1})	Reaction time (min)	Yield (%)[a]
1	1	0.451	30	55
			135	91
2	2.5	0.956	30	77
			60	95
3	5	1.897	30	98
4	10	3.118	30	52
			120	83
5	15	3.540	30	40
			270	87

Reaction conditions: benzaldehyde (2 mmol), Aniline (2 mmol), Ni/PVSA/CMK-3 (0.1 g), H_2O (3 mL), $NaBH_4$ (6 mmol), room temperature

[a]Isolated yield after work-up

PVSA/CMK-3 as an acid–metal catalyst was perused in water at room temperature and the outcomes are as follows.

Various quantities of $NiCl_2{\cdot}6H_2O$ were tested to clarify the impact of nickel nanoparticles concentration on the reductive amination process. Hence, in order to prepare Ni/PVSA/CMK-3, first, the amount of $NiCl_2{\cdot}6H_2O$ is changed from 1 to 15 mmol g^{-1}. Next, the amount of supported nickel was measured by the Atomic Absorption spectroscopy technique (AAS), the details are tabulated in Table 2. It is obvious that the catalyst activity improved gradually by an increase $NiCl_2{\cdot}6H_2O$ from 1 to 5 mmol g^{-1}. Two probable pathways are described as mechanistic issues of reductive amination: In the first one, the carbonyl compound at first is activated by the acid sites of the catalyst which subsequently reacts with the amine to produce imine and next, the C=N bond of the imine is hydrogenated with $NaBH_4$ or molecular hydrogen (H_2) to

Table 4 Effect of solvent on the reductive amination reaction

Entry	Solvent	Reaction time (min)	Yield (%)[a]
1	Water	30	98
2	Ethanol	60	95
3	Methanol	45	95
4	Acetonitrile	9	98

Reaction conditions: benzaldehyde (2 mmol), aniline (2 mmol), Ni/PVSA/CMK-3 (0.1 g, 9.5 mol% Ni and 20 mol% acid sites), $NaBH_4$ (6 mmol) and solvent (3 mL) at room temperature

[a]Isolated yield after work-up

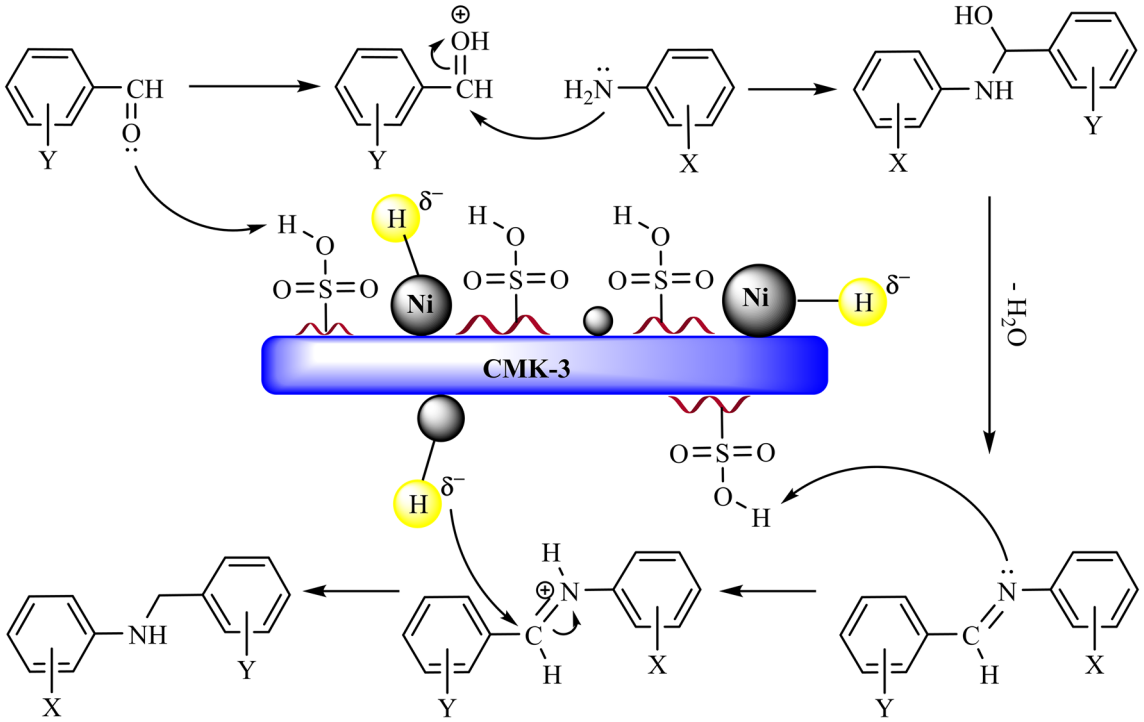

Scheme 2 A possible mechanism of one-pot reductive amination reaction over Ni/PVSA/CMK-3

Table 3 Effect of $NaBH_4$ amounts on the one-pot reductive amination reaction

Entry	Amount of $NaBH_4$ (mmol)	Reaction time (min)	Yield (%)[a]
1	0	300	0
2	4	30	43
		150	65
3	6	30	98
4	8	30	98

Reaction conditions: benzaldehyde (2 mmol), aniline (2 mmol), Ni/PVSA/CMK-3 (0.1 g, 9.5 mol% Ni and 20 mol% acid sites), $NaBH_4$ and H_2O (3 mL) at room temperature

[a]Isolated yield after work-up

Table 5 Effect of catalyst amount on the reductive amination reaction

Entry	Acetonitrile solvent			Water solvent		
	Amount of catalyst (g)	Reaction time (min)	Yield (%)[b]	Amount of catalyst (g)	Reaction time (min)	Yield (%)[a]
1	0.1	9	98	0.1	30	98
2	0.08	14	98	0.08	35	98
3	0.06	17	98	0.06	35	95
4	0.04	22	97	0.04	40	95
5	0.02	64	95	0.02	70	80

Reaction conditions: benzaldehyde (2 mmol), aniline (2 mmol), Ni/PVSA/CMK-3 and solvent (3 mL) at room temperature

[a]Isolated yield after work-up

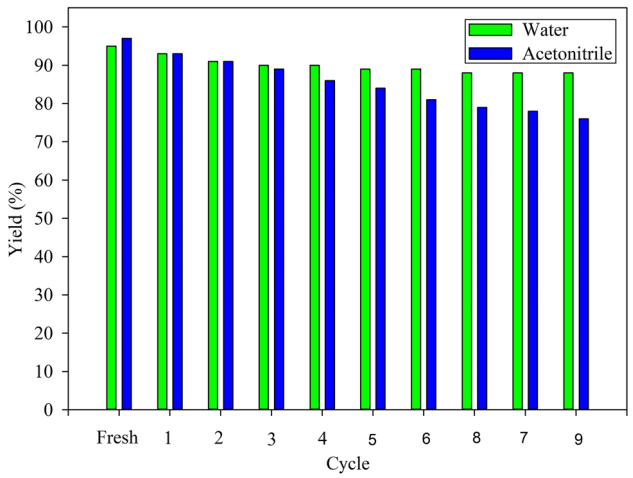

Fig. 11 The catalyst reusability for one-pot reductive amination reaction in acetonitrile and water solvents

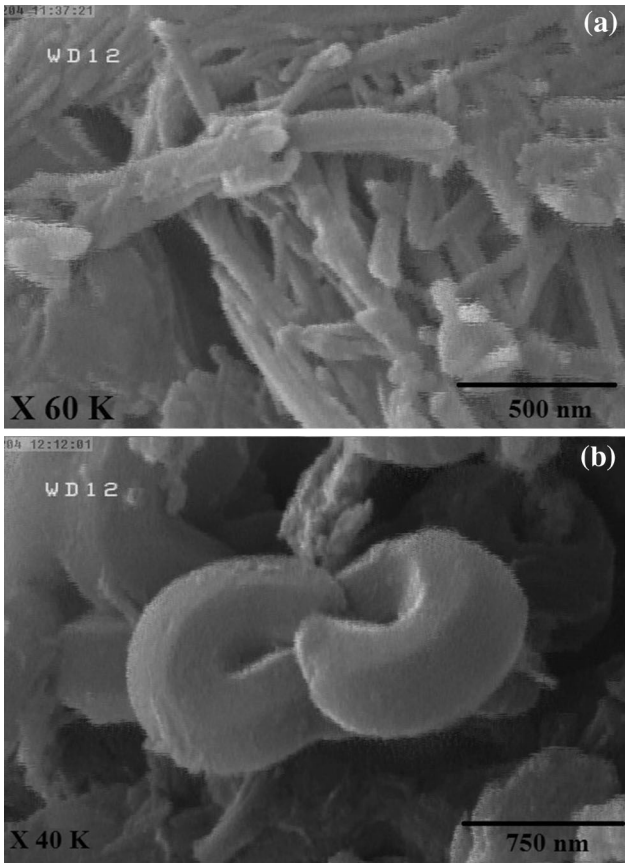

Fig. 12 Scanning electron microscopy (SEM) photographs of the used Ni/PVSA/CMK-3 catalysts in acetonitrile (**a**) and water (**b**) after the fifth run of the recycle reaction

yield the secondary amine (Scheme 2) [4, 42]. In the second, the benzaldehyde is hydrogenated with $NaBH_4$ or molecular hydrogen (H_2) to yield the benzyl alcohol which is converted to benzyl cation on acid sites of the catalyst and finally, it reacts with an amine to produce a secondary amine [4]. According to the possible catalytic reaction mechanism, nickel nanoparticles shift the mediated hydrides from BH_4^- ions to the iminium ions intermediates (Scheme 2) [43]. Subsequently, the volume of H^- on the catalyst surface is grown by intensifying nickel nanoparticles. Thus, the greatest quantity of hydrides could be conveyed to imine groups throughout the catalyst [2, 11]. The catalyst activity is slowed by a continual increase in $NiCl_2{\cdot}6H_2O$ (more than 5 mmol g^{-1}), this phenomenon could be assigned to the fact that the larger amount of nanoparticles are loaded on the surface of porous after an increase in a certain amount of nickel chloride. In fact, the nanoparticle size will increase by a boost in the quantity of $NiCl_2{\cdot}6H_2O$ [44, 45]; therefore, in some places, the pore size will narrow to a point that would enable lowering reactants diffusion rate into catalyst pores. Thus, lower performance of the catalyst is anticipated with higher $NiCl_2{\cdot}6H_2O$ concentration. Nevertheless, it does not imply completely pores obstruction. According to these consequences, the catalyst provided by 5 mmol g^{-1} $NiCl_2{\cdot}6H_2O$ presents the ideal catalytic activity.

To identify the effect of the $NaBH_4$ amount on the one-pot reductive amination (as a hydride donor), the reaction was carried out using various amounts of $NaBH_4$ in the

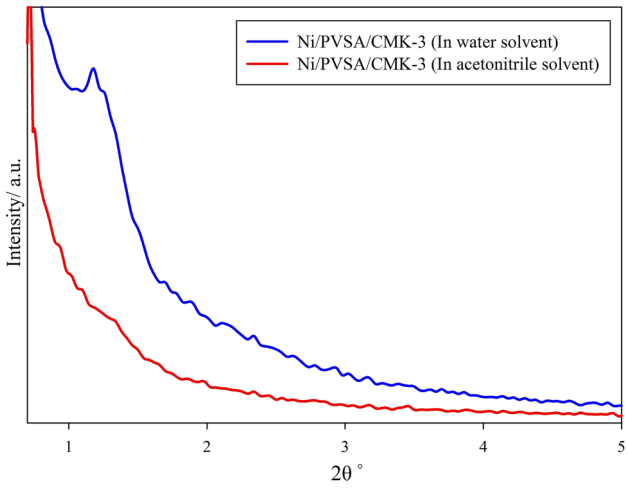

Fig. 13 XRD patterns of the used Ni/PVSA/CMK-3 after the fifth run of the recycle reaction in acetonitrile and water

presence of Ni/PVSA/CMK-3 as the catalyst. As observed in Table 3, in the absence of $NaBH_4$, no reductive amination product was observed. However, the yield is increased by rising $NaBH_4$ amount (up to 6 mmol). The excess values do not have any effects on this reaction. As a result, 6 mmol $NaBH_4$ is chosen in reductive amination reaction.

The impact of the solvent on the catalytic activity was assessed by the reductive amination reaction using Ni/PVSA/CMK-3 catalyst and $NaBH_4$ as a hydride donor, at room temperature. The findings are tabulated in Table 4. Four types of solvents: water, ethanol, methanol, and acetonitrile are tested. The most yield in low time is observed in acetonitrile and water. Moreover, the reaction time in acetonitrile solvent is lower than water. This could be due to the more hydrophobicity nature of acetonitrile solvent than water, which can dissolve aniline and benzaldehyde better. In addition, the hydrophobicity nature of acetonitrile is in proper harmony with the catalyst. The high reaction rate is observed in water which can be described by appropriate dissolving of $NaBH_4$ in water. In fact, the transformation of hydride ion (H^-) is well carried out in water. On the contrary, methanol and ethanol solvents have lower dielectric constants than water and hydrophobicity nature than acetonitrile. Thus, the reaction rates in these two solvents are lower than that of water and acetonitrile. In this context, water and acetonitrile were eventually nominated as the solvents for reductive amination reaction due to being environment-friendly and having high efficiency, respectively. All other optimizations and reactions have been accomplished by these two solvents in a separate manner.

The efficacy of Ni/PVSA/CMK-3 volumes is expressed in reductive amination reaction, Table 5. As observed, the reaction time increases by a reduction in the catalyst quantity from 0.1 to 0.04 g. Because the synthesized catalyst is expensive, it is decided to choose 0.04 g of the catalyst to react with the reactants. It should be noted that 0.02 g of the catalyst is insufficient to complete the reaction.

The catalyst reusability was surveyed by using Ni/PVSA/CMK-3 in water and acetonitrile solvents (Fig. 11). After each cycle, the catalyst was filtered off, washed with ethanol and water. Later, the catalyst was exposed at 60 °C and then reused in the reductive amination process with new reaction substances. After each run, a slight amount of the catalyst was lost in the filtration process; therefore, to overcome this obstacle, after each experiment, the amount of remained Ni/PVSA/CMK-3 was specified, and the molar ratio of the reactants was adjusted according to the remained catalyst. Ni/PVSA/CMK-3 was reused up to ten cycles. The results indicate that the catalyst in acetonitrile has serious activity loss of (21% decrease in activity after 10 runs), while the Ni/PVSA/CMK-3 recovery is much better in water (7% decrease in activity after 10 runs). The acidic site of the reused catalyst is measured 3.8 mmol g^{-1}, explaining that after the reaction process, the catalyst held their acidic nature. The stability of the catalyst can be justified by the fact that first, poly(vinylsulfonic acid) and CMK-3 have high molecular weight, and high surface area, respectively, which leads to enormous Van der Waals interaction between the CMK-3 backbone and polymeric

Table 6 Effect of catalyst for the one-pot reductive amination reaction

Entry	Catalyst	Acetonitrile solvent		Water solvent	
		Reaction time (min)	Yield of amine (%)[a]	Reaction time (min)	Yield of amine (%)[a]
1	Without catalyst	100	10	100	10
2	CMK-3	100	10	100	10
3	PVSA/CMK-3	60	40	70	35
4	Ni/PVSA/CMK-3	22	97	40	95

Reaction conditions: benzaldehyde (2 mmol), aniline (2 mmol), catalyst (0.04 g, 3.8 mol% Ni and 8 mol% acid sites), $NaBH_4$ (6 mmol) and Solvent (3 mL) at room temperature

[a]Isolated yield after work-up

Table 7 One-pot reductive amination of aldehyde compounds with aniline compounds over Ni/PVSA/CMK-3

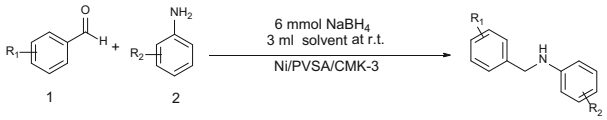

Entry	1	2	Product[a]	acetonitrile solvent			water solvent		
				Yield (%)[b]	Time (min)	TON/TOF (h^{-1})[c]	Yield (%)[b]	Time (min)	TON/TOF (h^{-1})[c]
1			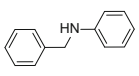	97	22	25.6/70	95	40	25/37
2			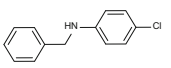	98	5	25.8/309	96	5	25.3/ 303.6
3			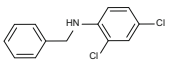	96	7	25.3/216	95	10	25/150
4			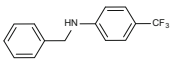	87	7	22.9/196	85	8	22.4/168
5		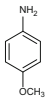	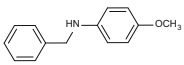	97	35	25.6/44	95	65	25/23
6	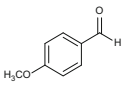		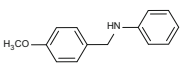	95	70	25/21	92	120	24.2/12
7			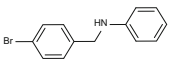	97	15	25.6/102	96	30	25.3/51
8			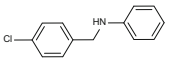	97	10	25.6/153	98	20	25.8/155
9	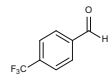		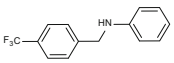	92	10	24.2/145	92	15	24.2/97
10	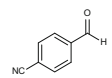		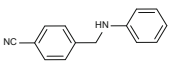	94	8	24.8/186	93	12	24.5/122
11	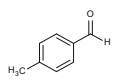		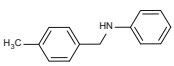	96	40	25.3/38	97	70	25.6/22
12			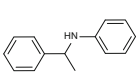	94	45	24.8/33	95	75	25/20
13			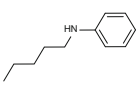	95[d]	17	25/88.4	95[d]	35	25/42.9
14				96[d]	12	25.3/126.5	95[d]	20	25/75.1
15				86[d]	35	22.7/38.9	83[d]	50	21.9/26.2
16[e]				98[d,f]	15[f]	25.8/103.3 [f]	98[d,f]	20[f]	25.8/77.5 [f]

Table 7 (continued)

Reaction conditions: aldehyde compound (2 mmol), amine compound (2 mmol), $NaBH_4$ (6 mmol), Ni/PVSA/CMK-3 (0.04 g, 3.8 mol% Ni and 8 mol% acid sites) and H_2O or acetonitrile as solvent (3 mL) at room temperature

[a]All synthesized compounds are known

[b]Isolated yield after work-up

[c]Turn-over number (mol product/mol Ni) and turn-over frequency (mol product/(mol Ni.h))

[d]Determined by GC

[e]Reaction between aldehyde and imine has not been observed

[f]Reduction of imine (N-butylpentan-1-imine)

carbon chains. Second, oxygen bonds in the structure of polymer chains interact with π bonds in the CMK-3 structure, which causes an increase in the connection between CMK-3 and PVSA. Finally, the monomers become polymerized into the micro and meso pores of CMK-3 through an in situ method and that polymeric chains cannot easily leach from the pores.

XRD and SEM analyses were accomplished to provide more appropriate assessments of the reused catalyst structure. The SEM images of the fresh and reused catalyst after 10 recycles in water and acetonitrile are displayed in Fig. 12, where the reused catalyst in water is completely stable and has the same morphology as that of the fresh catalyst (Fig. 12b). In contrast, the reused catalyst (after 10 recycles) in acetonitrile has a different morphology indicating the catalyst is destroyed (Fig. 12a). These results are compatible with XRD outcomes from the reused catalyst in water and acetonitrile (Fig. 13). Obviously, the symmetry of the reused catalyst in water is still intact with the same structure as the fresh catalyst, while the XRD plot does not show the ordered structure of CMK-3 in the acetonitrile where the specific peak around $2\theta = 1.04°$ is eliminated. It can be assumed that acetonitrile does not have a perfect adjustment with Ni/PVSA/CMK-3 nanocomposite, which leads to catalyst destruction. Because the reusability of a heterogeneous catalyst is a fundamental feature, water is chosen as the appropriate able solvent for reductive amination over Ni/PVSA/CMK-3.

The reductive amination reactions were accomplished to compare the catalytic activity of Ni/PVSA/CMK-3, CMK-3, PVSA/CMK-3, and without the catalyst. The sequels are tabulated in Table 6. The findings affirm the significant role of the acid–metal heterogeneous catalyst in reductive amination reaction. As shown in Table 6, the reaction does not advance more than 10% without the catalyst. It is important that $NaBH_4$ functions as a mild hydride donor agent, which is an incapable reagent for reducing imine groups solely. Similar results were obtained by consuming CMK-3 because mesoporous carbon CMK-3 does not have any active sites to carry out the reaction. By adding PVSA in CMK-3, the acidic feature of the mesoporous carbon increases; subsequently, the carbonyl group is activated. Thus the yield moderately increased from 10 to 40% and 35% in acetonitrile and water solvent, respectively. In addition, by using Ni/PVSA/CMK-3, the reaction efficiency is increased to about 95% in 22 and 40 min in acetonitrile and water solvents, respectively; because of the synchronous role of acidic and metallic sites to activate the carbonyl group of aldehydes and transfer hydride ions from $NaBH_4$ to the imine group, respectively.

Heterogeneous nature is an interesting feature in catalyst assessment. In this context, first, the catalyst was separated from the reaction mixture in the middle of reaction (50% conversion) by filtration and then centrifugation. Next, the reaction advance was monitored in the filtrate circumstance (data not shown). An unexpected improvement in the reaction is shown (approximately 15%) in the acetonitrile solvent after filtration of the catalyst at 50% conversion. This finding indicates that the catalyst is somewhat destroyed in acetonitrile and a small quantity of Ni nanoparticles leach into the solvent. Subsequently, the reaction continues in a homogeneous manner. This leaching is not evident even at a larger time in the water. This experiment reveals that in addition to having high Van der Waals interaction between the polymer and CMK-3, the monomers are completely polymerized into the pores. Thus, the polymers could not leach simply from the CMK-3 structure. To prove this claim, HPLC and AAS were accomplished to measure PVSA and Ni from the reaction solution, respectively. No significant amounts of PVSA and Ni have been observed in solution. Indicating that the nature of the reaction process in water is completely heterogeneous and homopolymer and nickel leaching do not occur.

Subject to optimization of the reaction conditions, the reaction was expanded to different benzaldehydes and anilines substitutes range (Table 7). The reactions were examined in water and acetonitrile solvent at 25 °C and the outcomes are displayed in Table 7. As observed, the reaction rate increases in presence of electron-withdraw groups including Cl, Br, CN, and CF_3 on benzaldehyde. The carbonyl group of benzaldehyde is more activated by the electron-withdraw group making the aniline attack to benzaldehyde easier. Thus, the formation of iminium ion is

more convenient [46]. An unexpected increase in the reaction rate by electron-withdraw groups in aniline is observed. Producing the intermediate of iminium salt is easier in the presence of electron-withdrawing groups in aniline and aldehyde and increase the possibility of H^- attack to iminium salt (Scheme 2) [47]. Based on the measured TOF and TON, the catalyst shows high activity at low temperature. In brief, there are several reasons why Ni/PVSA/CMK-3 shows this level of performance in mild conditions: First, the heterogeneity of the polymer is improved by using CMK-3; thus, the catalyst becomes more heterogeneous through this method; second, both high surface area of CMK-3 and the large amount of the polymer in pores leads to an increase in the nickel nanoparticles stabilizing. Furthermore, the nickel nanoparticles cannot aggregate in the pores of CMK-3; third, these systems (mesostructure) do not allow nickel nanoparticles to grow too much due to having specific pore diameter, which controls the size of nickel nanoparticles; fourth, the reactants easily pass through the pores of the catalyst due to hydrophobic nature of PVSA/CMK-3 and fifth, the synergic effect of acid and metal sites increase the carbonyl activation and hydrides transfer.

Conclusion

Nickel nanoparticle immobilized on mesoporous poly(vinylsulfonic acid)/CMK-3 is synthesized as an extremely effective heterogeneous catalyst. This acid–metal bifunctional catalyst demonstrates great efficiency in one-pot reductive amination reaction from aldehyde and amine in water and acetonitrile at room temperature. The catalyst simply is filtered from the process and it exhibits high stability and activity after ten cycles in water. The catalyst is not highly heterogeneous in acetonitrile, while it is heterogeneous in the water. In a similar sense, the reusability of the catalyst is better in water than acetonitrile and the catalyst is more stable in water. The existence of electron-withdraw groups increase the secondary amine compounds in both aldehyde and amine compounds. The products with high purity and without by-product are produced and intricate separation methods are not adopted in purification.

Compliance with Ethical Standards

Conflict of interest The authors declare that they have no conflict of interest.

References

1. S. Gomez, J. A. Peters, and T. Maschmeyer (2002). *Adv. Synth. Catal.* **344**, 1037.
2. E. W. Baxter and A. B. Reitz (2004). *Org. React.* **59**, 1.
3. A. F. Abdel-Magid and S. J. Mehrman (2006). *Org. Process Res. Dev.* **10**, 971.
4. Y. Z. Chen, Y. X. Zhou, H. Wang, J. Lu, T. Uchida, Q. Xu, S. H. Yu, and H. L. Jiang (2015). *ACS Catal.* **5**, 2062.
5. M. Nasrollahzadeh and S. M. Sajadi (2016). *J. Colloid Interface Sci.* **464**, 147.
6. J. W. Park and Y. K. Chung (2015). *ACS Catal.* **5**, 4846.
7. C. C. Lee and S. T. Liu (2011). *Chem. Commun.* **47**, 6981.
8. M. H. Valkenberg and W. F. Holderich (2002). *Catal. Rev.* **44**, 321.
9. Q. Zhang, S. S. Li, M. M. Zhu, Y. M. Liu, H. Y. He, and Y. Cao (2016). *Green Chem.* **18**, 2507.
10. A. Saha and B. Ranu (2008). *J. Org. Chem.* **73**, 6867.
11. A. Rahman and S. B. Jonnalagadda (2008). *Catal. Lett.* **123**, 264.
12. R. Rajesh and R. Venkatesan (2012). *J. Mol. Catal. A Chem.* **359**, 88.
13. F. Alonso, P. Riente, and M. Yus (2008). *Synlett* **9**, 1289.
14. F. Alonso, P. Riente, and M. Yus (1998). *Tetrahedron* **54**, 1921.
15. D. Shah and H. Kaur (2014). *J. Mol. Catal. A Chem.* **381**, 70.
16. L. F. Giraldo, B. L. López, L. Pérez, S. Urrego, L. Sierra, and M. Mesa (2007). *Macromol. Symp.* **258**, 129.
17. O. Mazaheri and R. J. Kalbasi (2015). *RSC Adv.* **5**, 34398.
18. S. K. Jain, R. J. M. Pellenq, K. E. Gubbins, and X. Peng (2017). *Langmuir* **33**, 2109.
19. A. Eftekhari and Z. Fan (2017). *Mater. Chem. Front.* **1**, 1001.
20. M. Choi and R. Ryoo (2003). *Nat. Mater.* **2**, 473.
21. S. Jun, S. H. Joo, R. Ryoo, M. Kruk, M. Jaroniec, Z. Liu, T. Ohsuna, and O. Terasaki (2000). *J. Am. Chem. Soc.* **122**, 10712.
22. M. Colilla, F. Balas, M. Manzano, and M. Vallet-Regí (2007). *Chem. Mater.* **19**, 3099.
23. R. J. Kalbasi and O. Mazaheri (2016). *New J. Chem.* **40**, 9627.
24. J. He, K. Ma, J. Jin, Z. Dong, J. Wang, and R. Li (2009). *Microporous Mesoporous Mater.* **121**, 173.
25. T. Okayasu, K. Saito, H. Nishide, and M. T. W. Hearn (2009). *Chem. Commun.* **0**, 4708.
26. M. Erkartal, H. Usta, M. Citir, and U. Sen (2016). *J. Membr. Sci.* **499**, 156.
27. D. Li, J. Li, D. Mao, H. Wen, Y. Zhou, and J. Wang (2017). *Mater. Chem. Phys.* **189**, 118.
28. D. D. Jiang, Q. Yao, M. A. McKinney, and C. A. Wilkie (1999). *Polym. Degrad. Stab.* **63**, 423.
29. K. H. Wu, Y. R. Wang, and W. H. Hwu (2003). *Polym. Degrad. Stab.* **79**, 195.
30. R. J. Kalbasi and N. Mosaddegh (2011). *J. Solid State Chem.* **184**, 3095.
31. S. Chytil, W. R. Glomm, E. Vollebekk, H. Bergem, J. Walmsley, J. Sjoblom, and E. A. Blekkan (2005). *Microporous Mesoporous Mater.* **86**, 198.
32. H. Song, R. Rioux, J. D. Hoefelmeyer, R. Komor, K. Niesz, M. Grass, P. Yang, and G. A. Somorjai (2006). *J. Am. Chem. Soc.* **128**, 3027.
33. P. Dibandjo, F. Chassagneux, L. Bois, C. Sigala, and P. Miele (2005). *J. Mater. Chem.* **15**, 1917.
34. D. Brühwiler and H. Frei (2003). *J. Phys. Chem. B.* **107**, 8547.
35. S. Kim, B. K. Yoo, K. Chun, W. Kang, J. Choo, M. S. Gong, and S. W. Joo (2005). *J. Mol. Catal. A Chem.* **226**, 231.
36. R. Jana, T. P. Pathak, and M. S. Sigman (2011). *Chem. Rev.* **111**, 1417.
37. E. Levin, E. Ivry, C. E. Diesendruck, and N. G. Lemcoff (2015). *Chem. Rev.* **115**, 4607.

38. H. Wena, K. Yao, Y. Zhang, Z. Zhou, and A. Kirschning (2009). *Catal. Commun.* **19**, 1207.
39. O. Metin and S. Ozkar (2008). *J. Mol. Catal. A Chem.* **295**, 39.
40. R. J. Kalbasi and F. Zamani (2014). *RSC Adv.* **4**, 7444.
41. R. J. Kalbasi, N. Mosaddegh, and A. Abbaspourrad (2012). *Appl. Catal. A Gen.* **78**, 423–424.
42. R. J. Kalbasi and O. Mazaheri (2015). *Catal. Commun.* **69**, 86.
43. M. A. Harrad, B. Boualy, L. El Firdoussi, A. Mehdi, C. Santi, S. Giovagnoli, M. Nocchetti, and M. Ait Ali (2013). *Catal. Commun.* **32**, 92.
44. Y. Zhai, Y. Dou, X. Liu, S. S. Park, C. S. Ha, and D. Zhao (2011). *Carbon* **49**, 545.
45. S. E. Bozbag, L. C. Zhang, M. Aindow, and C. Erkey (2012). *J. Supercrit. Fluids* **66**, 265.
46. N. Uday Kumar, B. Sudhakar Reddy, V. Prabhakar Reddy, and R. Bandichhor (2012). *Tetrahedron Lett.* **53**, 4354.
47. R. P. Tripathi, S. S. Verma, J. Pandey, and V. K. Tiwari (2008). *Curr. Org. Chem.* **12**, 1093.